Quantitative temperature measurements in high-pressure flames with multiline NO-LIF thermometry

Tonghun Lee, Wolfgang G. Bessler, Helmut Kronemayer, Christof Schulz, and Jay B. Jeffries

An accurate temperature measurement technique for steady, high-pressure flames is investigated using excitation wavelength-scanned laser-induced fluorescence (LIF) within the nitric oxide (NO) A–X(0, 0) band, and demonstration experiments are performed in premixed methane/air flames at pressures between 1 and 60 bars with a fuel/air ratio of 0.9. Excitation spectra are simulated with a computational spectral simulation program (LIFSim) and fit to the experimental data to extract gas temperature. The LIF scan range was chosen to provide sensitivity over a wide temperature range and to minimize LIF interference from oxygen. The fitting method is robust against elastic scattering and broadband LIF interference from other species, and yields absolute, calibration-free temperature measurements. Because of loss of structure in the excitation spectra at high pressures, background signal intensities were determined using a NO addition method that simultaneously yields nascent NO concentrations in the postflame gases. In addition, fluorescence emission spectra were also analyzed to quantify the contribution of background signal and to investigate interference in the detection bandwidth. The NO-LIF temperatures are in good agreement with intrusive single-color pyrometry. The proposed thermometry method could provide a useful tool for studing high-pressure flame chemistry as well as provide a standard to evaluate and validate fast-imaging thermometry techniques for practical diagnostics of high-pressure combustion systems.

OCIS codes: 120.1740, 120.6780, 300.2530, 280.2470.

1. Introduction

Temperature is one of the key quantities in combustion. It governs reaction chemistry (reaction rates and equilibrium states) and pollutant formation processes. In practical systems, accurate and precise determination of temperature allows optimization of combustor efficiency, as well as minimization of pollutant emissions. Temperature in flames and nonreacting flows can be determined by probe techniques,[1] but these potentially perturb the reactive flow and affect reaction chemistry. Other diagnostic methods include laser-based nonintrusive spectroscopic techniques[2,3] as reviewed by Stricker[4] and Laurendeau.[5] Spectroscopic methods either rely on population dependence of different rotational, vibrational, or electronic states of the target atom or molecule [spontaneous Raman scattering, laser-induced fluorescence (LIF), coherent anti-Stokes Raman scattering (CARS), absorption spectroscopy) or exploit the change of density, utilizing ideal gas arguments to obtain temperatures (Rayleigh scattering, spontaneous Raman scattering). CARS (Refs. 6 and 7) typically provides the highest accuracy but is experimentally complex and produces only single-point measurements. Laser absorption methods[8] are generally limited to line-of-sight integrated measurements. Rayleigh scattering[9,10] is relatively simple to implement but requires knowing the local gas composition (i.e., the effective scattering cross section). In addition, unfiltered Rayleigh scattering suffers from elastic scattering off surfaces and Mie scattering by particles. Spontaneous Raman scattering[11] is robust against scattering effects; however, signals are weak, and spectrally resolved detection is often required for accurate analysis, in which case 2D imaging becomes difficult. LIF (Ref. 12) can potentially

T. Lee (tonghun@stanford.edu) and J. B. Jeffries are with the High Temperature Gasdynamics Laboratory, Mechanical Engineering Department, Stanford University, Stanford, California. W. G. Bessler is with IWR and H. Kronemayer is with PCI, Universität Heidelberg, Heidelberg, Germany. C. Schulz is with IVG, Universität Duisberg-Essen, Duisburg, Germany.

Received 18 February 2005; revised manuscript received 24 May 2005; accepted 25 May 2005.

0003-6935/05/316718-11$15.00/0

yield spatially resolved images of the selected target species, but it often requires detailed spectroscopic parameters such as fluorescence yield, quenching, energy transfer, etc. for precise measurements. Although these spectroscopic techniques have been widely applied to combustion research, an accurate fast-imaging temperature measurement technique for practical high-temperature and high-pressure combustion systems is still an elusive target and a topic for further investigation. Our own efforts to enable such practical imaging based on rigorous spectroscopic studies of NO, O_2, and CO_2 UV-LIF in high-pressure flames are currently ongoing. The motivation for this study is to provide a validation tool for development of such fast-imaging techniques and for detailed study of high-pressure flame chemistry by enabling accurate and spatially resolved temperature measurements in steady systems. The work presented here complements our group's earlier work[13–15] to understand the influence of high pressure on NO-LIF measurements in flames. This earlier work focused on the optimum excitation or detection strategies for LIF measurement of NO concentration. Here we extend this work to optimize the use of NO-LIF for temperature in high-pressure flames.

The basic concept of this study involves fitting excitation spectra obtained from LIF of NO with simulation data to obtain temperatures. The technique was recently evaluated by Bessler and Schulz[16] for atmospheric flames, and the subsequent applications in spray flames and sooting flames up to 5 bars have verified its accuracy.[17,18] Unfortunately, the approach used at these lower pressures requires adjustments for high-pressure flame conditions ($p \leq 60$ bars). Our main objective in the current work is to extend multiline NO-LIF thermometry to high-pressure applications, to identify the main problems caused by the elevated pressure, and to provide a new protocol for data collection. The LIF temperatures in this study are compared with temperatures inferred from an intrusive single-color pyrometer measurement of a metal bead probe. In addition, the potential of this thermometry technique for spatially resolved measurements is demonstrated with a 1 D temperature profile along the path of the laser.

2. Multiline NO-LIF Thermometry at High Pressure

The multiline NO-LIF thermometry presented here is based on an excitation scan of laser wavelength over a number of lines in the rotational manifold of the NO A–X(0, 0) transition; this spectrum is then fit using a numerical spectral simulation to extract temperature. Multiline thermometry has also proved to be robust against elastic scattering from surface or particles, as well as against broadband LIF from polycyclic aromatic hydrocarbons (PAHs) and CO_2 (Ref. 19) or laser-induced incandescence (LII) from soot.[20] Although NO-LIF multiexcitation strategies have been previously applied to low pressure flames,[21] atmospheric pressure flames[22,23] and in an arc-jet reactor,[24] the first use of entire NO-LIF excitation spectra (NO A–X(0, 0) band) for temperature measurements in high-pressure flames was by Vyrodov *et al.*[25] in 1995, where accurate thermometry was demonstrated in flames up to 20 bars.

Here, we extend to high pressures ($p \leq 60$ bars) the NO-LIF multiline thermometry strategy of Bessler and Schulz,[16] for which the NO excitation spectrum is calculated for given fit temperature using LIFSim (Ref. 26) to account for the collisional broadening and interference for oxygen. Here we discuss specific problems caused by the elevated pressure (i.e., interference issues, signal attenuation, NO reburn, etc.), statistical sensitivity analysis for optimizing data-acquisition parameters, analysis of new data acquired with the new protocol, and the implementation of a more flexible computational fitting routine to allow flexible control over individual fitting parameters. Most important, the accuracy and applicable pressure range of this multiline thermometry technique is quantitatively assessed. An important practical problem is the careful determination of the LIF signal in the absence of NO (or the baseline), and this is discussed here in detail. Because the data acquisition requires a wavelength scan, the technique as presented is only applicable to steady combustion and flow systems or to repetitive systems in which phase-locked sampling is possible.

LIFSim (Ref. 26) is used for computational modeling of the NO and O_2 spectroscopy and implements a full spectroscopic database of NO A–X term energies and oscillator strengths, including pressure broadening and collisional quenching. LIFSim is based on a nontransient three-level model of NO (1, ground level; 2, excited level; 3, rotational manifold in ground level). Fast rotational energy transfer (RET) is assumed between levels 1 and 3, which leads to continuous thermal equilibrium, where a Boltzmann distribution is assumed for the ground-state population. Additional RET and vibrational energy transfer (VET) processes[27] are not considered in the version used in the current study.

The LIF excitation scan range used in this study extends from 225.944 to 226.112 nm (Fig. 1). It is a compromise between temperature sensitivity, applicable excitation scan range, data-acquisition time and suppression of interference signal from other species. The spectral region covers 40 NO rotational transitions that are blended into 14 distinct features at atmospheric pressure. This scan region is sensitive over a wide range of ground-state energies extending from room temperature to 3500 K. At higher pressures, the spectrum is significantly altered by collisional broadening (overlap of rotational lines) and shifting[28] as demonstrated by the NO excitation spectrum at 20 bars in Fig. 1. This altering produces a general reduction in intensity leading to a reduced signal-to-noise ratio (SNR). Therefore, it is important to implement a computational model that can accurately account for these phenomena. NO A–X transitions in high-pressure combustion gases also suffer from interference by other species, most notably LIF from multiple vibrational bands of O_2 (Ref. 29) and broadband CO_2 LIF (280–400 nm).[19] Simulated O_2-LIF excitation spectra are also shown in Fig. 1.

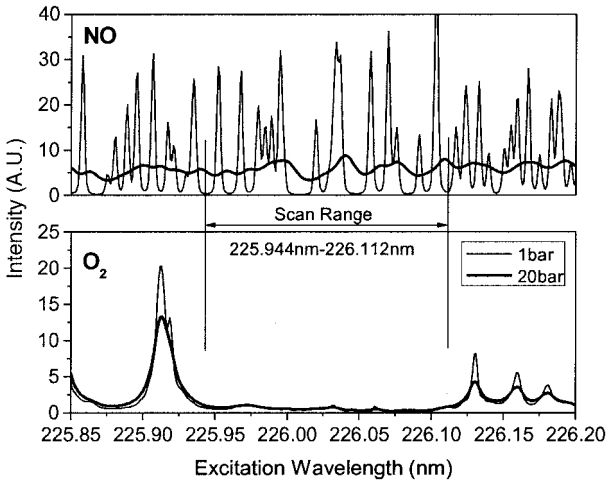

Fig. 1. Numerical simulation (LIFSim) of NO and O_2 LIF-excitation spectra in the range of 225.8–226.2 nm at 2000 K. The scan range (225.944–226.112 nm) is located in the region of minimum O_2 LIF interference. As spectra overlap caused by collisional broadening at 20 bars can be observed in the NO spectra, whereas O_2 is less affected because of predissociation. The intensities of NO and O_2 are on the same scale.

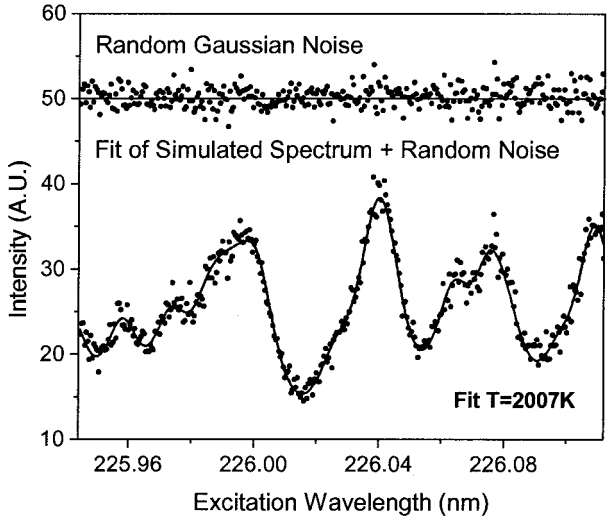

Fig. 2. Example of sensitivity analysis by using simulated spectra with added noise (Gaussian) and fitted to extract temperature at 20 bars (225.944–226.112 nm region). Random Gaussian noise is added to simulated spectra for temperature fitting to simulate experimental conditions.

The specific scan region in this study has been previously identified by DiRosa *et al.*[30] as having minimal interference from the *B–X* Schumann–Runge bands of O_2.[29] It can be seen that the entire scan region is void of any strong O_2 transitions.

The choice of optimal scan range and data-collection strategy is an important issue since applicable temperature range and temperature precision is influenced by these factors. To optimize temperature sensitivity, we extend the 1 bar analysis of Bessler and Schulz[16] and adapt a statistical analysis based on multiline fitting of simulated spectra with synthetic noise as shown in Fig. 2. The synthetic noise characteristics are chosen to reflect the noise of our detection system. The procedure is repeated 200 times times, and the standard deviation of the 200 fitted temperatures becomes a measure for the precision of the fitting technique. For a variety of starting wavelengths, pressures, scan ranges, and number of laser pulses averaged, the condition that provides minimal standard deviation is then identified as being the optimal scan range. For the precision and accuracy of the multiline thermometry method in this study, sensitivity analysis indicates that a local minimum in standard deviation of temperature exists around 226.03 nm where interference from O_2 is minimized (a global minimum exists around a scan origin of 225.22–225.47 nm, but is influenced by O_2 LIF). Additional simulations were carried out to assess the scan region length (Fig. 3), and the effect of varying the number of laser shots whose signal is averaged during data collection (Fig. 4) for different pressures. Although it is obvious that longer scan regions result in higher precision, Fig. 3 illustrates the relative increase in sensitivity with increased scan region. This information is used to determine the length of scan region for a target sensitivity. In the same way, Fig. 4 is used to determine the influence of on-chip averaging on temperature sensitivity. Both of these results indicate a loss of sensitivity with rising pressure due to declining SNR ratio. Target precision for the current thermometry was a subjective 5% (±100 K to 2000 K, horizontal bar in Figs. 3 and 4). While additional uncertainties in the experimental setup reduce the precision and accuracy in our results even further, statistical sensitivity analysis provides a theoretical

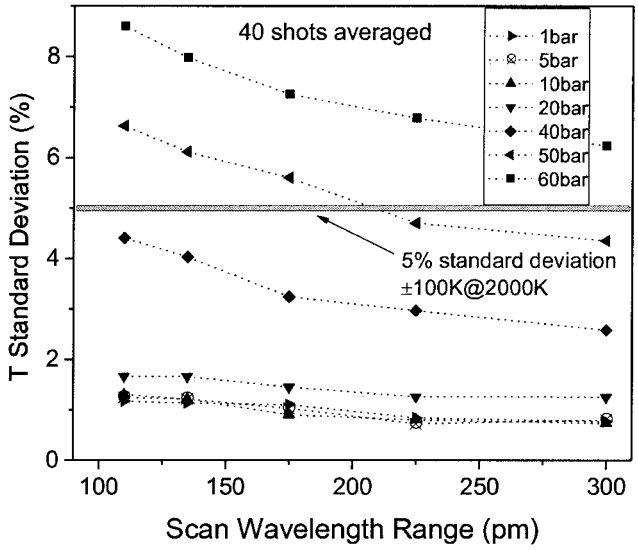

Fig. 3. Sensitivity analysis of temperature fitting with respect to scan wavelength range for 2000 K. The scan range centers around 226.03 nm (O_2-LIF suppression region). The signal from 40 laser pulses is averaged on a chip for each individual data point.

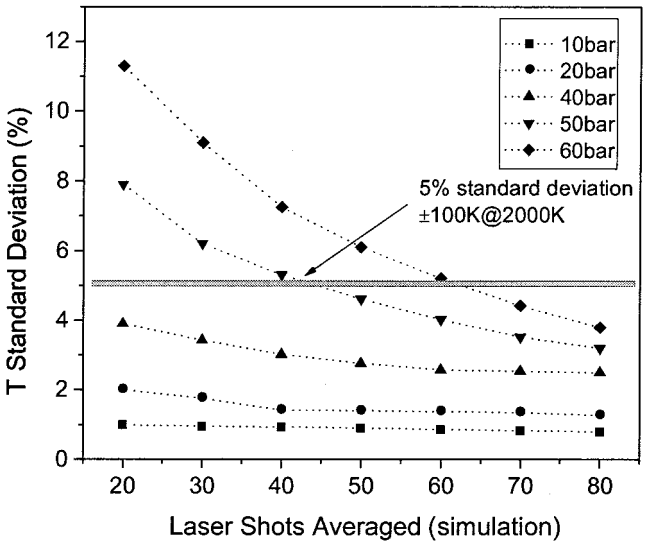

Fig. 4. Sensitivity analysis of temperature fitting with respect to the number of individual laser experiments that are averaged on a chip at each wavelength position for 2000 K. The scan range is 225.944–226.112 nm.

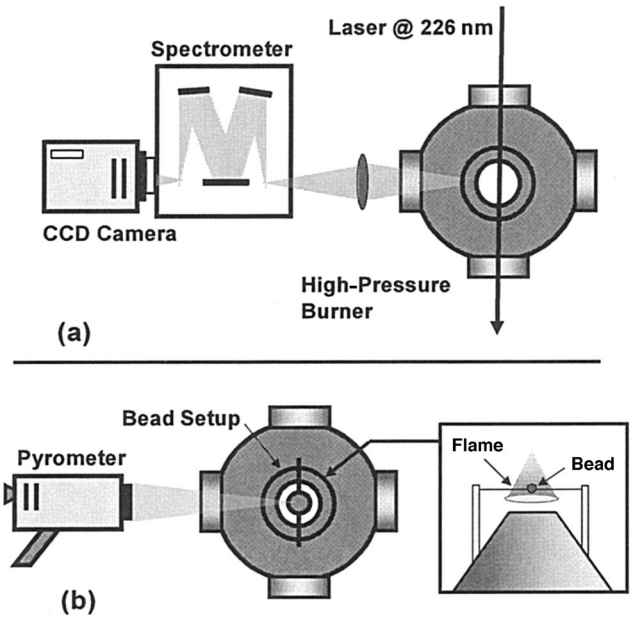

Fig. 5. Experimental setup (a) for NO-LIF multiline thermometry and (b) for an intrusive probe (Pt/Rh bead) infrared pyrometer measurement.

limit of performance, along with a guideline for use in the actual experiments.

3. Experimental Setup

Laminar, premixed methane/air flat flames at pressures from 1 to 60 bars were stabilized on a porous, sintered stainless-steel plate of 8 mm in diameter. This burner was mounted in a stainless-steel housing with an inner diameter of 60 mm with pressure stabilization of ± 0.1 bar.[15] Investigations were conducted for a $\phi = 0.9$ fuel/air equivalence ratio. An additional 2% (by volume) inert gas (N_2) was added to the feedstock gases to balance variable NO seeding at 400 ppm without changing the dilution of the burnt gases. Optical access to the flame was possible via four quartz windows (Heraeus, Suprasil 2 Grade). Laser pulse energy was 1 ± 0.2 mJ/pulse (7 ns pulse at 10 Hz) from a Nd:YAG-pumped (Quanta Ray GCR250) frequency-doubled (BBO) dye laser (LAS, LDL205). The beam was weakly focused (0.5 mm $\times$ 0.5 mm) along a line 3 mm above the burner matrix and crosses the flame horizontally [Fig. 5(a)]. The pulse energy was monitored with a fast photodiode (LaVision). Fluorescence signals were collected at right angles to the laser beam and focused with a $f = 105$ mm, $f/4.5$ achromatic UV-lens (Nikon), dispersed spectrally through an imaging spectrometer (LaVision Chromex 250IS) and imaged onto the chip of an intensified CCD camera (LaVision Dynamight) with a spatial resolution of 1024 $\times$ 1024 (CCD chip size). The spectrometer slit is aligned parallel to the laser beam and multiple laser shots are averaged on chip for each wavelength position. The resulting 2D image yields spatial resolution along one axis (8 mm) and emission wavelength (230–310 nm) on the other. Elastically scattered laser light was suppressed with a reflective dielectric filter (HR, FWHM 10 nm, centered around 226 nm, Laser Optik).

For the probe or pyrometer measurements, a platinum/rhodium (Pt/Rh) bead (0.5 mm diameter, Oriel type R bead) was suspended 4 mm above the flat flame in the postflame gas region [Fig. 5(b)]. Detection was via a single-color infrared pyrometer with measurement range of 600–3000 °C (Minolta-Land Cyclopes Model 152 Infrared Optical Pyrometer). The bead provided sufficient detection area for uniform emissivity in the lock-in zone of the pyrometer, and calibration of emissivity to blackbody radiation was performed at 1 bar using standard thermocouple measurements. Heat transfer calculations show that conduction losses from the bead to the base of the matrix via the suspension wire and subsequent convection from relatively cold coflow can account for at most a temperature difference of 15 K.

4. Data Evaluation

The multiline NO-LIF thermometry technique, in principle, has the potential for imaging measurements with a detection bandpass selected with filters in front of the camera.[16] However, in this paper we acquire spectrally resolved measurements with 1D spatial resolution along the laser line over the range of 230–310 nm. This arrangement allows us to monitor the quality of NO LIF and to assess interference and background signals by other species. It also allows flexible control of the detection bandpass for future data evaluation. For each point in the excitation scan, the camera collects an image with the spatial resolution along the horizontal path of the laser beam on the vertical axis and spectrally resolved emission spectra on the horizontal axis (Fig. 6). Data

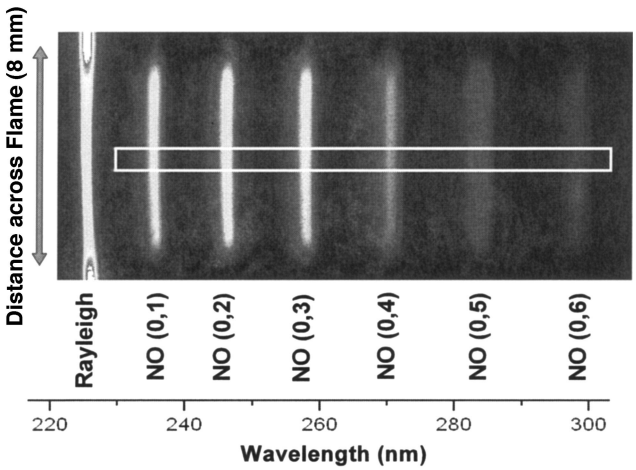

Fig. 6. Raw image, scan from a camera at an individual point of excitation (p = 20 bars, λ_{ex} = 226.034 nm). The white box in the center shows detection region for reconstruction of laser excitation spectrum (detection region is broadband 230–310 nm).

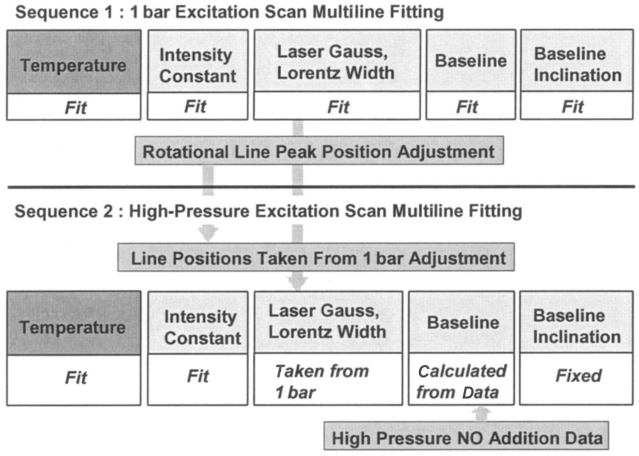

Fig. 7. Schematic of a multiline fit routine. Sequence 1 (upper) fits all parameters to determine the laser line shape and line positions. Sequence 2 (lower) extracts temperature with a reduced number of fit parameters.

from multiple laser shots are integrated on the CCD chip of the detection camera and then corrected by the average laser intensity. The laser pulse is absorbed in the hot gases by NO, CO_2, H_2O, and O_2,[31] of which the dominant absorption is by CO_2. At the highest pressures, 40% of the laser light is absorbed in the 8 mm path across the burnt gases. We estimate this laser energy perturbs the flame temperature by less than 20 K for the 1 mJ/pulse (10 Hz) used. The absorption of the subsequent LIF signal is at most 20% for the fluorescence of NO A–X(0, 0) and less for our redshifted detection band.

In the current study, the laser is scanned from 225.944–226.112 nm in steps of 0.001 nm, resulting in 168 individual image sets for each scan. The number of laser shots averaged at each wavelength position was increased from 20 to 80 with increasing pressure (1 to 60 bars), respectively to compensate for the reduction of SNR. An excitation spectrum is then extracted by spatially averaging a broadband detection region in the center of the imaged line (the box in Fig. 6 shows the 0.7 mm wide section that is spatially averaged in the middle of the flame). For NO LIF, the spectral shape of the emission spectra depends strongly on the rotational level to which the NO is excited.[32] Branching ratio (fluorescence versus RET rate and quenching rate) arguments suggest that while significant RET is observed, RET rates within the NO A ($v' = 0$) fail to completely redistribute the population in the initially populated state to neighboring states within the fluorescence lifetime. This means that the excited-state population distribution during emission is not in thermal equilibrium. Broadband detection therefore is preferred since it is insensitive to these nonuniform excited-state population distribution effects. Dependence of temperature accuracy on variation of detection bandpass is an ongoing issue for investigation.

Numerical calculations of NO excitation spectra are fitted to experimental data via a nonlinear least-square-fitting routine (Levenberg–Marquardt algorithm[33]). Measurements in a 1 bar flame are used to reduce the number of free parameters needed to fit the high-pressure data. The laser line shape (combination of Gaussian and Lorenzian terms) and exact position of the excitation lines are fixed to the values found in the 1 bar fits. The peak position of each excitation line is adjusted with the 1 bar data to account for inaccuracies in the spectroscopic database and experimental shortcomings of the laser tuning. The spectroscopic database is updated accordingly. The remaining pressure-dependent simulation parameters are temperature (our target parameter), signal strength (gain), and baseline signal (defined here as all signal in addition to NO LIF). A schematic of the entire procedure is shown in Fig. 7. Sequence 1 (upper) shows fitting of all parameters in a 1 bar flame to extract laser line shape and line positions. Sequence 2 (lower) then fits high-pressure data with a reduced number of fit parameters as well as new line positions determined from the 1 bar case.

A critical factor for determination of temperature in the high-pressure flame is the exact assessment of the contribution of the baseline signal strength. An example of a typical emission spectrum with NO A–X(0, 0) excitation is shown in Fig. 8 for 10 and 40 bars. Note that the signal caused by elastically scattered laser light overlaps the observed NO A–X(0, 0) LIF signal. Our detection region extends from 230 to 310 nm where LIF contribution from other species interferes with that of NO. For fuel lean flames studied here, the majority of the interference in the high temperature burnt gases is LIF from O_2. The fluorescent lifetime of the relevant excited states of O_2 are limited by predissociation, and therefore the pressure influence on line broadening and fluorescence quantum yield is much smaller than for NO and leads to an increase of the relative contribution of O_2-LIF background with increasing pressure. Although the excitation scan range avoids strong

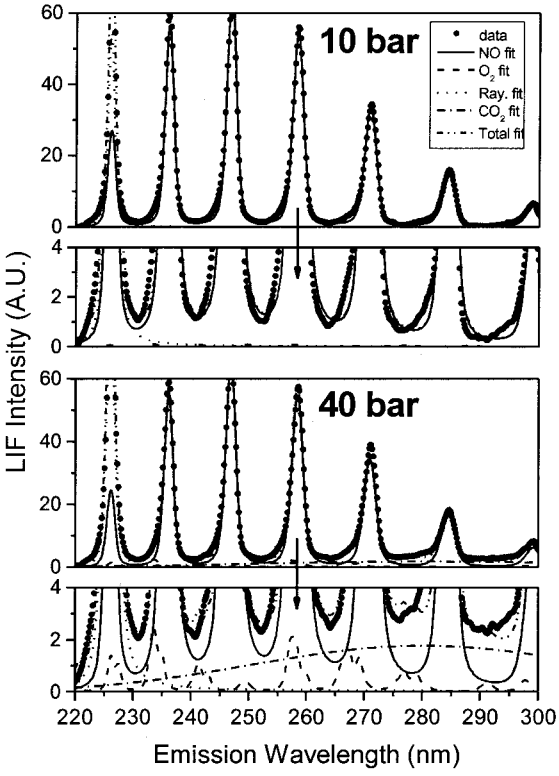

Fig. 8. LIF fluorescence spectrum with NO A–$X(0, 0)$ excitation at 10 and 40 bars. The spectrum is separated into contributions from different components (NO, CO_2, and O_2 LIF, Rayleigh scattering). The lower part of each plot is magnified for a clearer view of the spectral separation. The baseline is defined as sum of all signals in the detection region (230–310 nm), excluding NO LIF. λ_{ex} = 226.034 nm (400 ppm NO seeding, ϕ = 0.9).

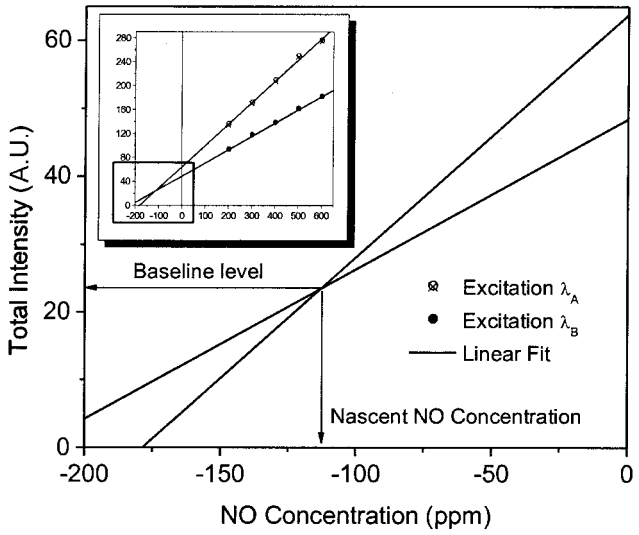

Fig. 9. NO addition method for the determination of the baseline strength and the nascent NO concentration at p = 30 bars. The plot shows a magnified view of the small box in the inserted graph. The NO addition is varied from 200 to 600 ppm, and NO LIF is detected with excitation at two different wavelengths. Excitations A and B refer to two different excitation wavelengths (λ_A, 226.03 nm; λ_B, 226.042 nm).

transitions of O_2, the relative interference from O_2 LIF does increase with pressure. In addition, the absorption and subsequent fluorescence from hot CO_2 (Ref. 19) increases with pressure and becomes a major contribution to the baseline at pressures above 20 bars. The relative increase of O_2 and CO_2 interference and subsequent contribution to the baseline can be observed in the 40 bar data in Fig. 8. Since collisional broadening of the NO transitions causes overlapping of neighboring lines during excitation (Fig. 1), there is no off-resonant position between excitation features for high-pressure conditions, and this complicates evaluation of the baseline. The nascent NO concentration in the flames is needed to evaluate this baseline, which is then used as a fixed parameter in the multiline fitting of the high-pressure data.

We determine the nascent NO concentration in the flame using a variable NO seeding method and later compare the nascent NO determined to values from multiparameter fitting of the fluorescence spectra. The LIF is measured at two different excitation wavelengths, which have minimal and maximum NO signal strengths, as illustrated in Fig. 9. These wavelengths are selected relatively close together in the target scan range where the baseline intensity can be assumed to be constant for a given pressure [region of minimal O_2 interference[30] and constant CO_2 LIF (Ref. 19)]. After the total signal at two different wavelengths at several different NO seeding concentrations is measured, the overall signal is linearly fit as a function of NO seeding for each of the excitation wavelengths. These two linear fits are extrapolated to their intersection, yielding the nascent NO concentration and the value of the baseline signal. This method is used to determine the baseline level for each flame as a function of pressure and ϕ. Determination of the nascent NO concentration (and LIF baseline) by this method assumes the NO reburn mechanism is first order in NO concentration. If this assumption was grossly in error the variation with NO seeding in Fig. 9 would not be linear. In the stoichiometric and lean flames studied here with less than 100 ppm NO addition, the NO reburn is expected to be linear in NO concentration and less than 10%.[34–36] We have also determined experimentally that the temperature in our flames does not vary ($\leq$5%) for NO additions as large as 1500 ppm, thus we expect the NO formation to be relatively independent of the NO seeding.

5. Results and Discussion

The baseline determination via the NO addition method (discussed above, cf. Fig. 9) is shown in Fig. 10 for 10, 20, 50, and 60 bar flames. NO was excited at two different wavelength positions (λ_A, 226.03 nm; λ_B, 226.042 nm) while the NO concentration was varied from 200 to 600 ppm in 100 ppm intervals. Two linear fits to the data converge in the lower, left quadrant and provide the baseline and nascent NO concentrations. As pressure approaches 60 bars, the slope of the two lines becomes nearly the same, and determination of the convergence point becomes dif-

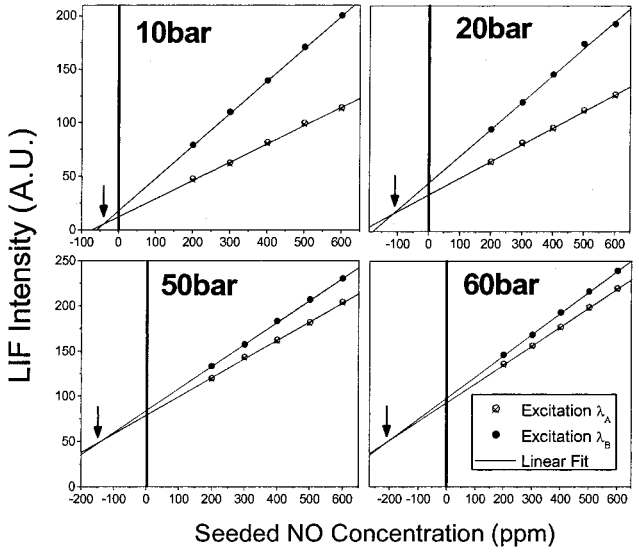

Fig. 10. NO addition plots for determination of baseline strength at 10, 20, 50, and 60 bars. Two lines in each graph are linear fits to the two different excitation wavelengths. Excitations A and B refer to two different excitation wavelengths (λ_A, 226.03 nm; λ_B, 226.042 nm).

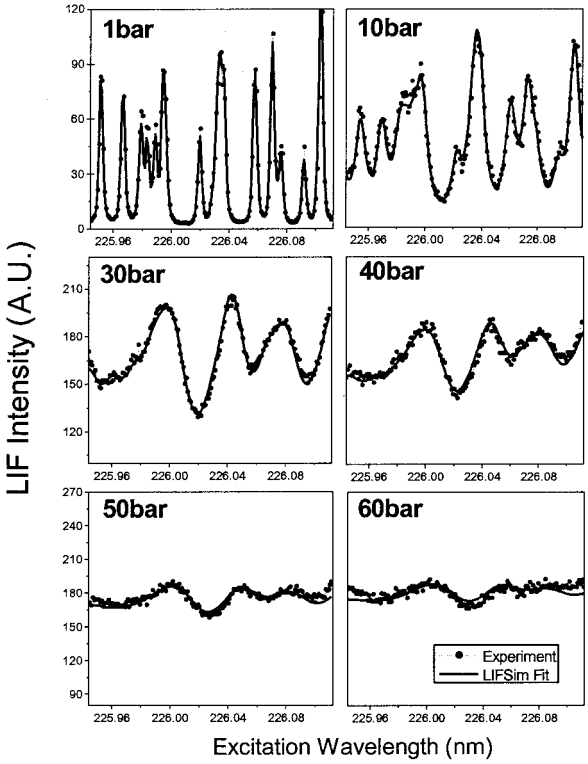

Fig. 11. Multiline temperature fitting in 1–60 bars, $\phi = 0.9$ CH_4/air flames (NO seeding at 400 ppm). The LIF-intensity scales of the 30, 40, 50, and 60 bar figures have been magnified for viewing clarity.

ficult. Subsequently, the extrapolation errors increase. The analysis assumes a constant baseline throughout the entire scan region, and careful correction is needed to match LIF intensity from the NO addition method with the intensity from a specific excitation wavelength of the laser in the excitation spectra, since the baseline contribution to the total signal (baseline/total signal) depends on the excitation wavelength of the laser. Note that strong structured O_2 LIF is avoided in this region (Fig. 1),[29] whereas an increased excitation region would require a variable baseline to account for the excitation-wavelength dependence of O_2. The baseline signal strength is inferred from the y axis (LIF Intensity) and used as a constant during the fit.

The result from the multiline temperature fitting for the 1 bar case and higher pressures (CH_4/air flame at $\phi = 0.9$) are shown in Fig. 11. For the 1 bar plot, none of the fitting parameters were fixed in the analysis procedure, yielding a laser Gaussian FWHM of 0.21 cm^{-1} and a Lorenztian FWHM of 0.03 cm^{-1}, in good agreement with laser specifications. In addition, the observed spectral positions of the absorption features (overlapping rotational lines) were compared with simulated data, and adjustments were made to the spectral line database. NO seeding was 400 ppm; a sufficient number density to provide large NO-LIF signal but small enough not to perturb flame dynamics or temperature.[16] The experimental reproducibility was confirmed by fitting ten repeating scans ($\Delta T = 40$ K). Additionally, 1 bar scans were conducted at the start and end of each day to check for drift in laser wavelength and for reproducibility of temperature results. The fitting results for higher pressures in Fig. 11 illustrate that the simulation can reproduce the experimental data very well. As the pressure increases, more laser pulses were averaged to compensate for the decrease of temperature sensitivity illustrated in Fig. 4, resulting in increasing data-collection times (e.g., 6 min data-acquisition time at 1 bar at 60 bars). Typical computational time for the fit was approximately 35 s (3 GHz Pentium III-PC), and this time is reduced by the use of a spectral database reduced to cover only the transitions in the scan region.

Figure 11 also shows the effect of collisional line broadening on the excitation spectra and deterioration of the SNR. Spectral overlap also reduces the number of NO peaks with increasing pressure, reducing the sensitivity of temperature to the spectral fit. In addition, baseline contribution is enhanced at high pressures owing to increased contribution from hot O_2 and CO_2 LIF. As for the applicable pressure range, we find that the fitting of this NO-LIF excitation region works well until 50 bars (though slight discrepancies occur at the edges of the scan range at 50 bars). The data at 60 bars illustrate that this scan region is inadequate to provide good temperature sensitivity at higher pressures owing to its loss of structure. The problem is compounded by low signal levels, possible minor inaccuracies in the assumptions of gas composition, potential inaccuracies in the spectral model, and difficulties in accurate baseline determination for high-pressure fitting. Unfortunately, increasing the scan range increases the excitation-wavelength-dependent contribution from

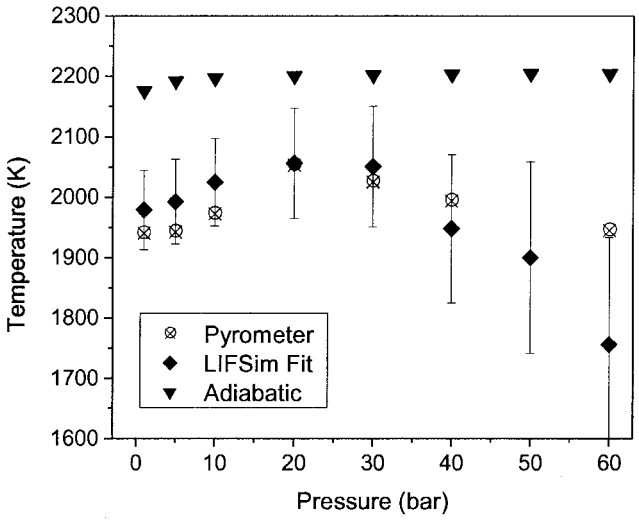

Fig. 12. Temperature versus pressure for the two different measurement techniques (multiline fitting, pyrometer). Adiabatic temperatures have been calculated by using the thermal equilibrium model (Stanjan[37]).

O_2 LIF. Investigation of the wavelength-resolved LIF data is underway to evaluate other detection bandpasses that can mitigate the O_2 contribution while maintaining the accuracy and precision of the fit.

Resulting temperatures obtained from the multiline fitting technique and pyrometer measurements are shown in Fig. 12. Temperatures are in good agreement within error range to 40 bars (e.g., ±72 K at 10 bars, ±91 K at 20 bars, ±120 K at 40 bars, ±180 K at 60 bars). The error here is a representation of statistical calculation taken from temperature sensitivity analysis (previously discussed in the section Multiline NO-LIF Thermometry at High Pressure) and additional uncertainties projected in our experimental setup or data processing procedures. As mentioned before, the quality of the fit starts to deteriorate at 60 bars and yields an underprediction of temperature in comparison with pyrometer measurements. In addition to general loss of structure in high-pressure spectra, O_2 transitions outside of our scan range can blend in because of collisional broadening (though weakened by predissociation) and disrupt our assumption of a uniform baseline. Adiabatic temperature in Fig. 12 have been calculated with a thermal equilibrium model, Stanjan.[37]

Apart from the NO addition method used in this study, there are other ways to determine the baseline. The baseline intensity can be extracted from the measured fluorescence emission spectra. As shown in Fig. 8, different overlapping contributions from LIF signals of NO, O_2, CO_2, and elastically scattered laser light can be numerically separated. The intensities of simulated NO- and O_2-LIF emission spectra, experimental CO_2-LIF emission spectra, and a Rayleigh-scattering signal can be simultaneously fit to wavelength-resolved experimental data via a nonlinear least-square-fitting procedure.[19] The background signal is then numerically integrated to yield the baseline intensity. While the NO addition approach is potentially applicable to 2D imaging setups, a spectrally resolved emission measurement is required for the emission spectra separation method, yielding at best 1D information. Alternatively, the baseline can be determined from a direct fit to the LIFSim simulation from which it is simply extracted from the multiline fitting routine as a free parameter (as done in 1 bar). Note this works well at 1 bar, where the structure of the spectra is well defined. Because of pressure broadening at high pressures ($p \geq 10$ bars), the scanned excitation wavelength range no longer contains off-resonance regions that allow the direct determination of background intensity, and the numerical fitting of the baseline becomes unstable. Comparison of baseline fraction (baseline signal/total signal) and subsequent temperatures for the different methods are shown in Table 1. Note that a shift in baseline intensity can produce a variation in the fit temperature even at pressures near 1 bar. An increase of baseline with pressure can be observed for constant excitation wavelength ($\lambda_{ex} = 226.03$ nm), owing to the increased contribution from hot O_2 and CO_2. For the NO addition method and the emission spectra separation, temperature differences are generally less than 70 K and within the error range of our thermometry method. However, baseline determination from direct multiline fitting results in temperatures that exhibit more deviation and that generally are outside our error range. While the emission spectrum analysis cannot be applied to 2D im-

Table 1. Comparison of Baseline Fraction (%) and Resulting Temperature from the NO Addition Method, Emission Spectra Method, and by Direct Baseline Determination from Multiline Fitting for Different Pressures[a]

	Pressure (bars)					
Baseline/Total Signal × 100(%)	10	20	30	40	50	60
NO addition method	2.5	6.8	12.1	14.9	24	26.5
Emission spectra separation	3.6	7.7	14.4	16.8	19.3	21.1
Baseline from direct fitting	6.5	12.2	14.7	24.3	28.8	58
Temperature (K)						
NO addition method	2025	2056	2051	1948	1900	1756
Emission spectra separation	2095	2089	2106	1984	1831	1693
Baseline from direct fitting	2279	2300	2115	2127	2067	2354

[a] $\lambda_{ex} = 226.034$ nm. Temperatures are from multiline fitting of excitation spectra with baseline determination from respective methods.

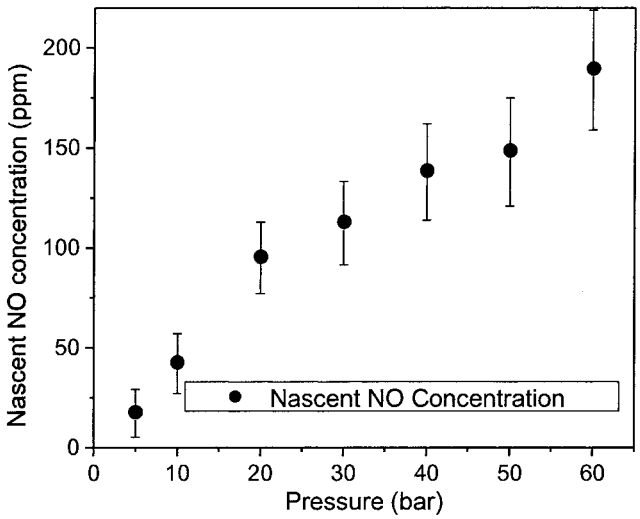

Fig. 13. Nascent NO concentration versus pressure. Concentrations are derived from the NO addition method.

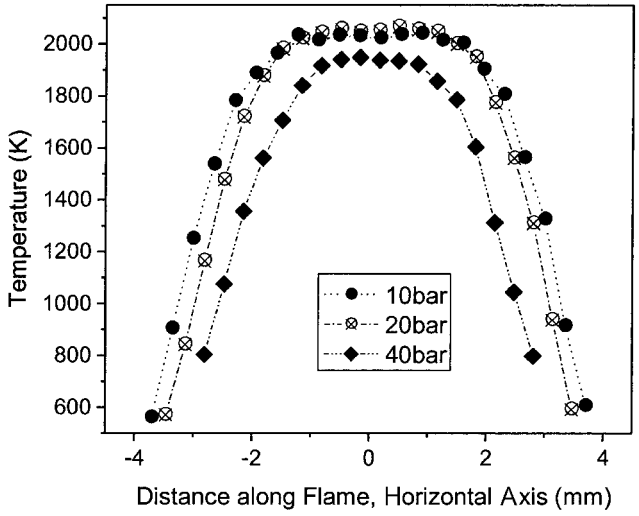

Fig. 14. Spatial temperature profile (1D) along a horizontal line in the flame (3 mm above burner matrix) for 10, 20, and 40 bars. $\phi = 0.9$ CH_4/air flame with 400 ppm NO seeding.

aging measurements, baseline contribution can be determined at much higher pressures than the NO addition method, which is limited by the rapidly converging convergence lines (Fig. 10) and can be useful in higher pressure regions where single point or 1 D line-resolved measurements are sufficient.

Figure 13 shows nascent NO concentrations calculated from the NO addition strategy as a function of pressure. Because of the high temperatures involved, the main NO formation mechanism is expected to be via the thermal NO formation (Zeldovich[38]). While the temperature decreases slightly with increasing pressure, an increase in NO concentration is observed with increasing pressure because of the dependence of the Zeldovich mechanism on gas density. In addition a slight increase in the prompt NO formation reactions, including that involving intermediate N_2O, can be considered, although the third body collision (proportional to pressure) requirements for N_2O formation is compensated by reduction of N_2O lifetime due to the high temperatures.[39]

Multiline thermometry has the potential for 2D imaging with an image recorded at each spectral position. This results in a 3D data structure with two spatial axes and one excitation-wavelength axis. For each pixel (corresponding to local flame position), the LIF excitation spectrum is extracted along the wavelength axis and evaluated with multiline thermometry. Then 2D temperature fields can be reconstructed from the individual fitting results. Higher-pressure applications are complicated by the fact that baseline contribution must be determined for each pixel position, and an elaborate calculation routine must be implemented to extract baseline for each location inside the flame. As a simplified demonstration, we present results of a temperature profile along a horizontal 1D line in our flame (Fig. 14) for 10, 20, and 40 bar flames. The spatial resolution comes from our spectrometer alignment where the beam is parallel to the slit and thus provides a line-resolved spectra in the direction of the laser. To account for the attenuation of the laser propagating through the medium, the baseline was determined separately for each individual spatial position using the NO addition method. The profiles show a plateau where the flat flame exhibits a constant temperature and rapid cooling near the edges. The coflow air was not seeded with NO, therefore the cold outer regions were not accessible with the NO-LIF technique. The smooth temperature profiles illustrate the robustness of this thermometry method, as well as demonstrate the potential to provide accurate spatially resolved temperatures.

6. Conclusion

We have demonstrated a robust multiline thermometry technique for application in steady high-pressure flames and have assessed the accuracy of the method. Temperatures are reported in a stable, premixed methane/air flame ($\phi = 0.9$) at pressures between 1 and 60 bars and are compared with an intrusive bead/pyrometer measurement for first-order comparisons. The technique combines the measurement of NO-LIF signals within a predefined spectral range with fitting of simulated spectra using the flexible computational tool LIFSim. While computational modeling compensates for spectral overlap caused by strong collisional broadening, severe reduction of SNR ratio limits the technique to applications at $p \leq 60$ bars. The method yields absolute, quantitative temperatures without the aid of an external calibration. The experiment has confirmed the LIFSim spectral database needed to investigate potential strategies for fast-imaging thermometry for high-pressure combustion applications. Potential applications include temperature validation for high-pressure flame chemistry and steady practical combustion systems. Multiline fitting can also serve as a validation protocol for evaluating the accuracy and precision of the new strategies for fast-imaging thermometry in laboratory conditions.

Work at Stanford was supported by the U.S. Air Force Office of Scientific Research, Aerospace Sciences Directorate, with Julian Tishkoff as the technical monitor. The Division of International Programs at the U.S. National Science Foundation supports the Stanford collaboration via a cooperative research grant. The University of Heidelberg work and the travel of WGB, HK, and CS are sponsored by the Deutsche Forschungsgemeinschaft (DFG) and the Deutsche Akademische Auslandsdienst (DAAD).

The authors especially acknowledge Ronald K. Hanson. The work was done in his laboratory with his support and scientific guidance. All of us have enjoyed our collaboration with Ron. He provides a congenial, collegial environment where scientific creativity is valued and rewarded. Ron encouraged and nurtured the long-standing collaboration between Stanford and Heidelberg/Duisburg. We thank Ron for his support of this work and wish him a very happy birthday.

References

1. M. V. Heitor and A. L. N. Moreira, "Thermocouples and sample probes for combustion studies," Prog. Energy Combust. Sci. **19,** 259–278 (1993).
2. A. C. Eckbreth, *Laser Diagnostics for Combustion Temperature and Species* (Gordon and Breach, 1996).
3. J. Wolfrum, "Lasers in combustion: from basic theory to practical devices," Proc. Combust. Inst. **27,** 1–41 (1998).
4. W. P. Stricker, "Measurements of temperature in laboratory flames and practical devices," in *Applied Combustion Diagnostics,* K. Kohse-Höinghaus and J. B. Jeffries, eds. (Taylor and Francis, 2002).
5. N. M. Laurendeau, "Temperature measurements by light scattering methods," Prog. Energy Combust. Sci. **14,** 147–170 (1988).
6. D. A. Greenhalgh, *Advances in Non-Linear Spectroscopy* (Wiley, 1988).
7. L. P. Goss, *Instrumentation for Flows with Combustion* (Academic, 1993).
8. R. K. Hanson, "Temperature measurement technique for high-temperature gases using a tunable diode laser," Appl. Opt. **17,** 2477–2480 (1978).
9. R. W. Dibble and R. E. Hollenbach, "Laser Rayleigh thermometry in turbulent flames," Proc. Combust. Inst. **18,** 1489–1499 (1981).
10. A. Orth, V. Sick, and J. Wolfrum, "Laser-diagnostic multispecies imaging in strongly swirling natural gas flames," Proc. Combust. Inst. **25,** 143–150 (1994).
11. A. Anderson, *The Raman Effect* (Marcel Dekker, 1971).
12. J. M. Seitzman, G. Kychakoff, and R. K. Hanson, "Instantaneous temperature field measurements using planar laser-induced fluorescence," Opt. Lett. **10,** 439–441 (1985).
13. W. G. Bessler, C. Schulz, T. Lee, J. B. Jeffries, and R. K. Hanson, "Strategies for laser-induced fluorescence detection of nitric oxide in high-pressure flames. I. *A–X*(0, 0) excitation," Appl. Opt. **41,** 3547–3557 (2002).
14. W. G. Bessler, C. Schulz, T. Lee, J. B. Jeffries, and R. K. Hanson, "Strategies for laser-induced fluorescence detection of nitric oxide in high-pressure flames. II. *A–X*(0, 1) excitation," Appl. Opt. **42,** 2031–2042 (2003).
15. W. G. Bessler, C. Schulz, T. Lee, J. B. Jeffries, and R. K. Hanson, "Strategies for laser-induced fluorescence detection of nitric oxide in high-pressure flames. III. Comparison of *A–X* excitation schemes," Appl. Opt. **42,** 4922–4936 (2003).
16. W. G. Bessler and C. Schulz, "Quantitative multi-line NO-LIF temperature imaging," Appl. Phys. B **78,** 519–533 (2004).
17. H. Kronemayer, I. Düwel, and C. Schulz, "Temperature imaging in spray flames," presented at the European Combustion Meeting (Louvain-la-Neuve, Belgium, 2005).
18. M. Hofmann, H. Kronemayer, B. F. Kock, H. Jander, and C. Schulz, "Laser-induced incandescence and multi-line NO-LIF thermometry for soot diagnostics at high pressures," presented at the European Combustion Meeting (Louvain-la-Neuve, Belgium, 2005).
19. W. G. Bessler, C. Schulz, T. Lee, J. B. Jeffries, and R. K. Hanson, "Carbon dioxide UV laser-induced fluorescence in high-pressure flames," Chem. Phys. Lett. **375,** 344–349 (2003).
20. M. Hofmann, W. G. Bessler, C. Schulz, and H. Jander, "Laser-induced incandescence (LII) for soot diagnostics at high-pressure," Appl. Opt. **42,** 2052–2062 (2003).
21. A. T. Hartlieb, B. Atakan, and K. Kohse-Höinghaus, "Temperature measurement in fuel rich non-sooting low-pressure hydrocarbon flames," Appl. Phys. B **70,** 435–445 (2000).
22. M. Tsujishita, A. Hirano, M. Yokoo, T. Sakuraya, and Y. Takeshita, "Accurate thermometry using NO and OH laser-induced fluorescence in an atmospheric pressure flame," JSME Int. J. Ser. B **42,** 119–126 (1999).
23. M. Yorozu, Y. Okada, and A. Endo, "Two dimensional rotational temperature measurement by multiline laser induced fluorescence of nitric oxide in combustion flame," Opt. Rev. **3,** 293–298 (1996).
24. E. A. Brinkman, G. A. Raiche, M. S. Brown, and J. B. Jeffries, "Optical diagnostics for temperature measurements in a dc arcjet reactor used for diamond deposition," Appl. Phys. B **64,** 689–697 (1997).
25. A. O. Vyrodov, J. Heinze, M. Dillman, U. E. Meier, and W. Stricker, "Laser-induced fluorescence thermometry and concentration measurements on NO *A–X*(0, 0) transitions in the exhaust gas of high pressure CH_4/air flames," Appl. Phys. B **61,** 409–414 (1995).
26. W. G. Bessler, C. Schulz, V. Sick, and J. W. Daily, "A versatile modeling tool for nitric oxide LIF spectra," in *Proceedings of the Third Joint Meeting of the U.S. Sections of The Combustion Institute*, Chicago, 16–19 March 2003, paper P105, http://www.lifsim.com.
27. J. W. Daily, W. G. Bessler, C. Schulz, V. Sick, and T. B. Settersten, "Nonstationary collisional dynamics in determining nitric oxide laser-induced fluorescence spectra," AIAA Journal **43,** 458–464 (2005).
28. M. D. DiRosa and R. K. Hanson, "Collision broadening and shift of NOγ (0, 0) absorption lines by O_2 and H_2O at high temperatures," J. Quant. Spectrosc. Radiat. Transfer **52,** 515–529 (1994).
29. G. Herzberg, *Spectra of Diatomic Molecules* (Krieger, 1950).
30. M. D. DiRosa, K. G. Klavuhn, and R. K. Hanson, "LIF spectroscopy of NO and O_2 in high-pressure Flames," Combust. Sci. Technol. **118,** 257–283 (1996).
31. C. Schulz, J. B. Jeffries, D. F. Davidson, J. D. Koch, J. Wolfrum, and R. K. Hanson, "Impact of UV absorption by CO_2 and H_2O on NO LIF in high-pressure combustion applications," Proc. Combust. Inst. **29,** 2725–2742 (2002).
32. C. Schulz, V. Sick, U. E. Meier, J. Heinze, and W. Stricker, "Quantification of NO *A–X*(0, 2) laser-induced fluorescence: investigation of calibration and collisional influences in high-pressure flames," Appl. Opt. **38,** 1434–1443 (1999).

33. W. H. Press, W. T. Vettering, S. A. Teukolsky, and B. P. Flannery, *Numerical Recipes in C: The Art of Scientific Computing* (Cambridge U. Press, 1992).
34. B. A. Williams, and J. W. Fleming, "Comparative species concentrations in CH_4/O_4/Ar flames doped with N_2O, NO and NO_2," Combust. Flame **98,** 93–106 (1994).
35. P. A. Berg, G. P. Smith, J. B. Jeffries, and D. R. Crosley, "Nitric oxide formation and reburn in low-pressure methane flames," Proc. Combust. Inst. **27,** 1377–1384 (1998).
36. J. H. Bromly, F. J. Barnes, S. Muris, X. You, and B. S. Haynes, "Kinetic and thermodynamic sensitivity analysis of the NO-sensitised oxidation of methane," Comb. Sci. Tech. **115,** 259–296 (1996).
37. W. Reynolds, *Stanjan: Chemical Equilibrium Solver* (Stanford University, 1987).
38. Y. Zeldovich, "The oxidation of nitrogen in combustion and explosion," Acta Physicochimica USSR **21,** 577–628 (1946).
39. C. T. Bowman, "Control of combustion-generated nitrogen oxide emission: technology driven by regulation," Proc. Combust. Inst. **24,** 859–878 (1992).